IEEE Open Access Journal of
Power and Energy

Received 31 August 2023; revised 1 December 2023; accepted 14 December 2023.
Date of publication 19 December 2023; date of current version 26 December 2023.

Digital Object Identifier 10.1109/OAJPE.2023.3344750

Robustness and Stability Analysis of Automatic Voltage Regulator Using Disk-Based Stability Analysis

PASALA GOPI[1], MEISAM MAHDAVI[2] (Senior Member, IEEE), AND HASSAN HAES ALHELOU[3] (Senior Member, IEEE)

[1]Department of Electrical and Electronics Engineering, Annamacharya Institute of Technology and Sciences, Rajampet 516115, India
[2]Department of Electrical Engineering, University of Jaén, Linares, 23071 Jaén, Spain
[3]Department of Electrical and Computer Systems Engineering, Monash University, Clayton, VIC 3800, Australia
CORRESPONDING AUTHOR: H. H. ALHELOU (alhelou@ieee.org)

ABSTRACT In this paper, the authors propose a novel design approach for the PID controller in the automatic voltage regulator (AVR) system using the Naked Mole Rat Algorithm (NMRA). The proposed algorithm has been extensively tested through MATLAB simulation studies. These studies have confirmed the effectiveness of the NMRA tuning method in achieving improved AVR system performance compared to the other tuning methods in the literature. In addition to performance evaluation, this article also investigates the robustness of the AVR system with an NMRA-tuned PID controller. This was achieved by conducting a disk-based stability analysis under model uncertainty. Also, the proposed NMRA-PID controller has a higher gain change tolerance than the TSA-PID controller for the given perturbations in the feedback loop of the AVR system for the specified values of disk size and skew. By studying the performance and robustness of the AVR system with an NMRA-tuned PID controller and comparing it with other techniques, this study provides insights into the benefits and capabilities of the proposed approach.

INDEX TERMS Naked Mole Rat algorithm, disk-based margins, robustness, model uncertainty, automatic voltage regulator.

ABBREVIATIONS AND NOMENCLATURE

A. ABBREVIATIONS

ANNs, dB	Artificial neural networks and decibel.
DPM, DGM	Disk phase margin and disk gain margin.
GM, PM	Gain margin and Phase margin.
NMRA,TSA	Naked mole rat and tree seed algorithm.
PID+D^2	PID plus second-order derivative.
HGSO	Henry Gas Solubility Optimization

B. PARAMETERS

b_p, e(s), f (t), f	Breeding probability, error signal, objective function, and multiplicative factor.
G_{min},G_{max}	Minimum and maximum gain.
K_a,K_{ex},K_g	Amplifier, exciter, and generator gain constant.
K_{vs},%Os	Sensor gain constant and overshoot percentage.
T_a,T_{ex},T_g	Amplifier, exciter, and generator time constant.
T_r,T_s,T_{vs}	Rise, settling, and feedback sensor time constant.
u,λ	Random numbers between 0 and 1.
u(s),y(s)	Input and output signal.
δ, ξ	Normalized uncertainty and damping factor.

I. INTRODUCTION

THE voltage profile in a power system is closely related to some important factors such as reliability, control, and power quality [1], and when it deviates from its desired level, it can result in various changes in the system dynamics and lifespan of electrical equipment connected to the grid [2], [3]. Some equipment such as sensitive electronic devices may be particularly vulnerable to voltage fluctuations. When the voltage profile deviates from its idle state, it can lead

to power surges or sags, which can damage or degrade the performance of these devices. Moreover, the rapid voltage drop can cause a sudden loss of power supply, resulting in disruptions in critical operations or processes. To mitigate these issues, power engineers employ various techniques and control mechanisms to regulate and stabilize the voltage profile of a power grid [4].

A. LITERATURE ON TUNING ALGORITHM

There are various types of controllers such as proportional (P), proportional + integral (PI), and proportional + integral + derivative (PID) which are commonly used in industrial operations [5]. The Ziegler-Nichols (ZN) technique is a simple approach for achieving an acceptable control performance for many systems. The ZN method furnishes an initial point for PID tuning and requires additional fine-tuning based on the requirements of system dynamics and performance. Also, this approach presumes a first-order plus time delay (FOPTD) model, which may not be suitable for all systems, especially those with complex dynamics or nonlinearities [6]. By tuning the PID controller, the system could respond to changes in the voltage profile and quickly adjust the excitation levels of the generator to maintain the desired voltage [7]. The combination of an Automatic Voltage Regulator (AVR) and PID controller allows for effective voltage regulation, helping to stabilize the voltage profile in the power system. This, in turn, ensures better power quality, improved grid reliability, and enhanced control over the system. In summary, maintaining a constant voltage profile in a power system network is crucial for the efficient operation of electrical equipment and overall system performance. The installation of voltage regulators, coupled with PID controllers, helps to address these challenges by actively regulating the generator terminal voltage and stabilizing voltage profile [8].

Tuning of optimal parameters for controllers in a plant is crucial for achieving the desired response. Various heuristic optimization techniques have been employed for this purpose. Heuristic optimization techniques are algorithms that do not guarantee an optimal solution but rather explore the search space to find good or near-optimal solutions. These techniques are well suited for controller tuning in AVR systems because they can handle the complexity and nonlinearity of the system while searching for an optimal parameter set. Particle Swarm Optimization (PSO) is a popular heuristic optimization technique for controller tuning. In AVR tuning, PSO can be used to find optimal values for the AVR parameters by iteratively adjusting the particle positions based on the fitness (performance) of the corresponding solutions [9], [10]. However, it suffers from limitations, such as slow convergence during the iterative process, local minima, and complexity in parameter selection. In a multi-area power system, the presented metaheuristic [11] is intended to dynamically improve the PID control gains for automated voltage and load frequency management. The inventive nonlinear search function and the nonlinear threshold acceptance algorithm enhance the control scheme's flexibility and efficiency. Ant Colony Optimization (ACO) can be employed to find optimal parameter values by simulating the pheromone deposition and trail following of ants [12]. In [13], Harmony Search (HS) was used for AVR tuning by representing the control parameters as musical notes. Fuzzy-logic-based AVR is a control system approach that utilizes fuzzy logic principles to control and regulate the output voltage, providing a flexible and intuitive framework for dealing with complex and uncertain systems [14]. Study [15] presented the application of ANNs and the Levenberg-Marquardt algorithm to establish the relationship between the voltage set point of the AVR system and the generator output voltage, offering a data-driven and accurate modeling technique for power systems analysis and control.

Study [16] investigated the performance of Archimedes Optimization Algorithm (AOA) for calculating the PID controller coefficients in AVR systems. The effectiveness of the AOA was validated in [13] by optimizing the coefficients of FOPID (Fractional Order PID) and PID+D^2 controllers. Reference [17] presented a novel metaheuristic algorithm, mRUN, which is an adaptation of the Runge Kutta optimizer with a modified opposition-based learning mechanism. This algorithm is then utilized for the optimization of the PID+D^2 controller in an AVR system. Study [18] involved a FOPID controller for a DC motor and an AVR system. The cutting-edge optimization algorithm (opposition-based hybrid slime mold with simulated annealing) is used to fine-tune the controller parameters. Also, [19] proposed a new technique that involves the HGSO algorithm to optimize the parameters of a FOPID controller for terminal voltage control in an AVR system. The effectiveness of the approach is demonstrated through box plots and convergence analyses, highlighting the efficiency of the optimization process.

A hybrid metaheuristic method was proposed for the optimal tuning of four types of PID controllers in AVR systems. The method combines the Manta Ray Foraging Optimization algorithm with a Simulated Annealing algorithm. The performance of this method was compared with other metaheuristic methods mentioned in [20]. In [21], an optimal Tree-Seed Algorithm (TSA)-based PID controller was proposed for tracking the terminal voltage of the AVR system, in which the performance of the TSA-based PID controller was compared with different metaheuristic optimization algorithms. In [22], the Whale Optimization Algorithm (WOA) technique was used to tune the parameters of AVR controllers. The performance of the AVR system was compared with various optimization algorithms such as Artificial Bee Colony (ABC) [23], Differential Evolution (DE), Harmony Search (HS), Teaching-Learning Based Optimization (TLBO), and Many Optimizing Liaisons (MOL).

Kalyan et al. [24] applied the Falcon Optimization Algorithm (FOA) for tuning the PID controller. In this regard, an Integral Double Derivative (IDD) controller was demonstrated and designed using Water Cycle Algorithm (WCA) in [25].

B. LITERATURE ON STABILITY ANALYSIS

The stability of the AVR system is paramount for ensuring reliable power supply, maintaining power quality, and facilitating the smooth operation of the entire power system. By regulating the terminal voltage of the power generation, the AVR system contributes significantly to system stability. In control systems, various techniques are available for assessing the stability of dynamic systems. One commonly used technique is the pole-zero map, which offers a straight forward way to analyze the system stability due to its simplicity [26]. Additionally, stability analysis in the frequency domain can be conducted by examining the conventional stability limits GM and PM, derived from the Bode diagram [27]. However, a limitation of the bode plot is its inability to provide the minimum GM and PM necessary for a comprehensive plant stability analysis. This article suggests that the disk-based stability analysis can mitigate the limitations of conventional methods. Compared with classical techniques [28], the disk-based stability approach offers enhanced insight into system stability, enabling engineers to gain a better understanding of the dynamic behavior and robustness of the control system. This provides a more rigorous analysis by considering both the gain and phase margins simultaneously, which leads to a stronger assurance of stability [29], [30].

C. RESEARCH GAP AND SOLUTION

The optimization of AVR systems is a complex and challenging task due to various factors such as complex system dynamics, nonlinear behavior, operational constraints, and uncertain conditions. Although there have been significant advancements in optimization techniques for AVR systems, there still exists a research gap in improving the set-point tracking performance of the AVR system. The development of new algorithms is an active area of research, and the introduction of a novel approach can potentially contribute to addressing the challenges in AVR optimization. The Naked Mole Rat algorithm (NMRA) is a newly introduced technique for tuning PID coefficients. This article suggests that NMRA can effectively tune PID coefficients and improve the performance of the AVR system. To evaluate the effectiveness of the proposed controller, the article compares it with other techniques for PID tuning. By comparing the performance of NMRA with these techniques, present paper aims to show the advantages and efficacy of the proposed technique.

In practical systems, there are deviations between the mathematical model and the actual system, particularly in terms of magnitude and phase. These deviations may arise due to uncertainties, nonlinearities, delays or other factors. In some cases, even if a system exhibits large classical margins, small combinations of gain and phase perturbations can lead to instability. This is because classical margins do not account for the simultaneous perturbations in both magnitude and phase. Disk-based margins offer an alternative approach to system analysis that takes into account these practical deviations and uncertainties. Rather than considering only a single point on the bode plot (as done in classical margins), disk-based margins take into account a region or disk in the plot. This region represents the uncertainty in the system's behavior at higher frequencies, where deviations from the mathematical model tend to be more significant. Please refer to Section IV for a more detailed explanation of desk-based margins.

D. CONTRIBUTIONS

The main key points of the contribution are:

- Naked More Rat Algorithm (NMRA) as a new optimization method is proposed for optimal PID controller tuning.
- The performance of the NMRA-PID controller is compared with those of the other controllers discussed in the literature.
- The model uncertainty used in this article, is the mismatch between the mathematical model and the actual system and is counted as complex perturbations in the feedback loop or multiplicative factor (f).
- With the use of disk-based stability analysis, the robustness of the suggested method on the AVR is examined, including its model uncertainty.
- The robustness of the controller obtained by the disk-based margins is compared with that of classical margins.

II. MODEL OF AVR SYSTEM

AVR is a device used in power systems to maintain a stable voltage output from a generator [31]. It is an essential component that helps regulation and control of the voltage within acceptable limits, ensuring the reliable and efficient operation of electrical equipment. AVR typically comprises control circuits, sensing elements, and an excitation system. The control circuit receives feedback signals from the voltage sensors and compares them to the desired voltage reference. Based on this comparison, the control scheme adjusts the generator field excitation, thereby regulating the output voltage of the generator. AVRs are commonly used in various applications, including power plants, industrial facilities, renewable energy systems, and backup power systems, where voltage stability and regulation are critical for the proper operation and protection of electrical equipment. Fig. 1 shows the connection of an AVR with power generation.

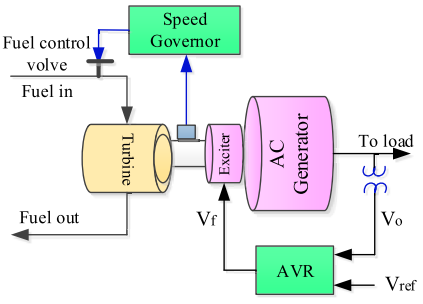

FIGURE 1. Connection of an AVR with power generation.

A. MODEL OF AVR SYSTEM COMPONENTS

To simplify the analysis and design of control schemes for AVR, it is required to linearize the nonlinear behavior of the AVR components around a specific operating point. This simplifies the mathematical representation and design control strategies. The AVR system typically consists of several components that each component is approximated as a first-order transfer function by considering its dynamic response [8], [32], [33]. The transfer function provides the relationship between the reference voltage (V_{ref}) and the excitation voltage (V_{ex}). The first order transfer function for an exciter is given by:

$$G_{ex}(s) = \frac{K_{ex}}{1 + s\tau_{ex}} \tag{1}$$

The first-order transfer function accounts for the dynamics of the exciter system, such as time delay and response curves.

The feedback control loop of the AVR system, which compares the generator output voltage (V_o) with the reference voltage (V_{ref}) and adjusts the excitation accordingly, is approximated as a first-order transfer function. This transfer function describes the control loop's dynamics, including the response time and stability characteristics.

$$G_{vs}(s) = \frac{K_{vs}}{1 + s\tau_{vs}} \tag{2}$$

The transfer function captures the dynamic behavior of the generator, including its response time and frequency characteristics. This can be derived from the mathematical modeling of the generator and its associated control system [32]. The first-order transfer function for a generator in an AVR system can be expressed as

$$G_g(s) = \frac{K_g}{1 + s\tau_g} \tag{3}$$

The amplifier in an AVR system is represented as a first-order transfer function by considering the relationship between the output signals of the amplifier and the voltage error signal [33]. The first-order transfer function for the amplifier in the AVR system can be expressed as:

$$G_a(s) = \frac{K_a}{1 + s\tau_a} \tag{4}$$

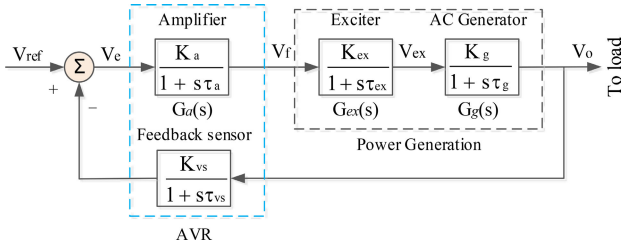

FIGURE 2. AVR with power generation – Block diagram.

The standard range and proposed values of the AVR system are given in [8] and [21]. Fig. 2 depicts a complete block diagram of the AVR with power generation.

From the block diagram, the transfer function of the AVR with power generation is given as [8].

$$G_{AVR}(s) = \frac{V_o(s)}{V_{ref}(s)} = \frac{0.1s + 10}{0.0004s^4 + 0.0454s^3 + 0.555s^2 + 1.51s + 11} \tag{5}$$

III. NAKED MOLE RAT ALGORITHM-BASED PID TUNING

Failing the AVR can result in losing the generator's excitation, which leads to a sudden decrease in the terminal voltage on the generator side. This situation can potentially damage the load or the consumers connected to the generator. To address this issue, a suitable PI or PID controller can be added to the AVR system. The controller would continuously monitor the generator's terminal voltage and adjust the excitation control signal to maintain the voltage within an acceptable range. An optimal controller can be designed by linearizing the components of the AVR system and using well-established control theory techniques. In this article, a new optimization method called the Naked More Rat algorithm (NMRA), is proposed for optimal controller tuning. NMRA is a nature-inspired algorithm that replicates the mating behaviors observed in NMRs. The NMRA has proven to be reliable, highly efficient, simple, and robust in its implementation with strong convergence properties when compared to other major algorithms in literature.

This algorithm is inspired by the social structure and reproductive dynamics of NMR colonies, where there are two distinct types of individuals: workers and breeders. During the worker phase, the workers put in constant effort to become breeders. This mimics the behavior of NMR workers who work diligently to gain reproductive status. The workers may engage in tasks or processes that contribute to the success and survival of the colony. In the breeder phase, the breeders compete with each other to mate with the queen. In the NMR colony, only a few selected individuals, known as breeders, are responsible for mating with the queen and producing offspring. The breeders strive to be chosen as the mating partners based on their ability to produce viable offspring. If a breeder becomes infertile or fails to meet the reproductive requirements, they are expelled from the breeder group and reassigned to the worker group. This expulsion ensures that only the most capable breeders remain in the breeding subgroup. As breeders are removed from their position due to infertility, the most physically fit worker is promoted to breeder status. This promotes a form of natural selection, where the fittest individuals are allowed to reproduce and pass on their genetic traits. There are three steps in the Naked More Rat algorithm: initialization, worker, and breeder [34].

Initialization: The population (n) of NMRs is randomly initialized, and each NMR is represented as a d-dimensional vector. Where d is the variable or parameter number. Each NMR is initialized as

$$NMR_{i,j} = NMR_{lb} + u(0, 1) * (NMR_{lb} - NMR_{ub}) \tag{6}$$

In (6), $NMR_{i,j}$ is the i^{th} solution of the j^{th} dimension. $i = [1, 2, 3 \ldots n]$, and $j = [1, 2, 3 \ldots d]$. NMR_{lb} and NMR_{ub} are the lower and upper limits of the function respectively. $u(0,1)$ is any random number (uniformly distributed) in the range 0 to 1. After initialization, the objective function and its fitness are evaluated. Breeder and worker NMRs are categorized according to the fitness values obtained, and the best NMR is chosen among these.

Worker: When the workers' fitness improves, they may have the opportunity to become breeders and mate with the queen. The fitness of the new NMR is calculated using

$$\omega_i^{t+1} = \omega_i^t + \lambda \left(\omega_j^t - \omega_k^t \right) \tag{7}$$

where ω_i^t be the i^{th} worker in the t^{th} iteration; ω_j^t and ω_k^t are the worker NMRs that are randomly chosen. λ (scaling factor) is any random number in search space [0 1]. ω_i^{t+1} denotes the new fitness solution. If mating fitness is better, the new solution for this new NMR is saved and the old solution is left out. All worker rats go through this procedure again, and each worker rat's final fitness is recorded.

Breeder: The breeder NMR should be physically fit to become a mating partner and stray as a breeder. Any breeder that is unfit for mating is regarded as a worker. The breeder NMR automatically updates based on the breeding probability (b_p) among the best d (i.e. variable or parameter). b_p is any random number in the range of [0, 1].

$$b_i^{t+1} = \left(1 - \lambda\right) b_j^t + \lambda \left(d - b_k^t\right) \tag{8}$$

Here, b_k^t is the i^{th} breeder of the t^{th} iteration. The parameter λ controls the mating frequency and is used to find the new breeder b_i^{t+1}.

A. IMPLEMENTATION OF ALGORITHM FOR PID TUNING

To apply the Naked Mole Rat (NMR) algorithm for PID controller tuning, the following steps were adopted:

Step-1: Initialization - Randomly initialize a population of NMRs (each NMR represents a PID set), maximum number of iterations (itr_{max}), dimensions, and breeding probability (b_p).

Step-2: Worker Phase - Evaluate the performance of each NMR (PID parameter set) and rank the NMRs based on their performance metric (Integral Time Absolute Error, *ITAE*). The performance of each NMR is estimated by minimizing the following objective function.

$$f(\mathrm{t}) = \min \int_0^\infty t \left| V_{ref} - V_o \right| dt \tag{9}$$

Step-3: Breeder Phase - Select the breeders based on their performance ranking, and determine the breeding pool. Apply genetic operators to create offspring solutions from the selected breeders. The offspring solutions represent new PID parameter sets.

Step-4: Evaluate Offspring - Measure and evaluate the performance of each offspring using the same performance metric as in the worker phase.

Step-5: Reassignment and Promotion - Identify any breeders who become infertile or fail to meet the performance criteria. Reassign these infertile breeders back to the worker group. Promotes the NMR with the best performance from the worker group to the breeder group, allowing it to contribute its parameters for future breeding.

Step-6: Termination Criteria - Set termination condition as reaching a maximum number of iterations. If the termination conditions are not met, repeat steps 2 to 5 iteratively. Once the termination conditions are met, select the best-performing PID parameter set based on the fitness evaluations conducted throughout the iterations.

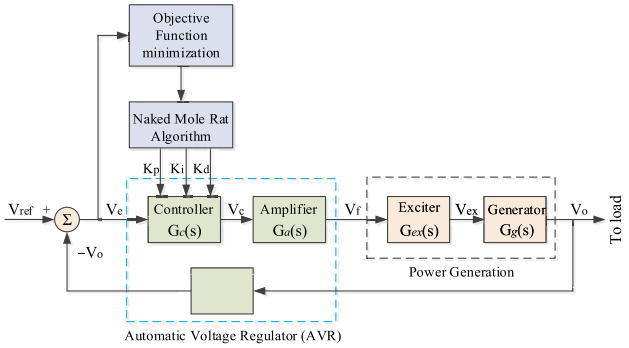

FIGURE 3. Implementation of NMR Algorithm.

Fig. 3 depicts the process of implementing the NMR algorithm on AVR system to obtain the PID coefficients. For the optimal coefficients of PID controller, the objective function (9) is minimized subjected to the following constraints: $K_{pmin} \leq K_p \leq K_{pmax}$; $K_{imin} \leq K_i \leq K_{imax}$; $K_{dmin} \leq K_d \leq K_{dmax}$ and for derivative filter time constant (t_f): $0 < t_f < 0.01$.

Because of the stochastic nature of this technique, 25 simulation runs were carried out to find the optimal PID coefficients. PID coefficients are likely represented by a three-dimensional solution space, and each run has a population size of 50 and a maximum of 100 iterations. The breeding probability is set at 0.5. The obtained PID coefficients are $K_p = 0.9487$, $K_i = 0.7096$, and $K_d = 0.3713$.

The convergence graph of NMRA and TSA is shown in Fig. 4. The figure makes it evident that the NMRA has superior fitness values over the TSA. Poor exploration and becoming trapped in local optima are two prevalent issues with Naked Mole Rat Algorithm. In order to find the best solutions, this algorithm randomly selects the value of b_p and λ to balance the exploration and exploitation.

IV. ROBUSTNESS AND STABILITY ANALYSIS

The transient response of any system determines its stability and is influenced by the delay margin (DM). The maximum time delay of a system before becoming unstable is known as the delay margin. In classical control theory, gain margin and phase margin are typically determined at a specific frequency point, such as the crossover frequency. These margins indicate how much the gain or phase can be increased

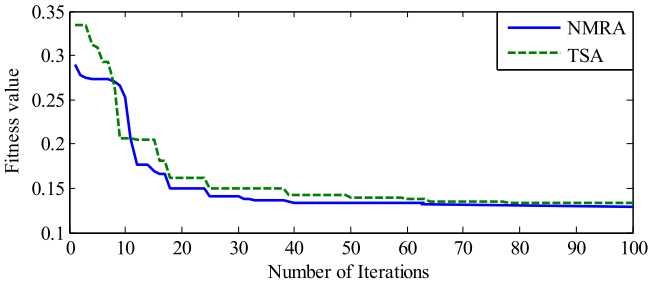

FIGURE 4. Comparison of performance of NMRA and TSA.

or decreased at that particular frequency before the system becomes unstable. On the other hand, Disk-based Gain Margin (DGM) and Disk-based Phase Margin (DPM) provide a more comprehensive analysis by considering all frequencies and loop interactions. They quantify the maximum amount by which the gain or phase can change across the entire frequency range without loss of stability, in absolute units and degrees, respectively. The DGM and DPM are related to an advanced method of stability analysis that considers all frequencies and loop interactions, providing a stronger guarantee of stability than classical gain and phase margins.

A. MODELING GAIN AND PHASE VARIATIONS

Consider a unity feedback system, comprising a plant (P) and a controller (C), as shown in Fig. 5. Both the plant and controller are assumed to be linear time-invariant (LTI) and single-input, single-output (SISO) systems. To introduce the mismatch between the mathematical model and the real system, a complex perturbation 'f' is used. This perturbation accounts for uncertainties or variations that can arise in practical systems. The loop transfer function, denoted as C^*P, represents the transfer function of the closed-loop system when the plant and controller are combined. The open-loop (L) represents the transfer function of the system without feedback connection.

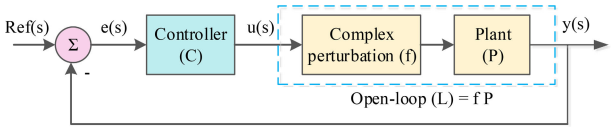

FIGURE 5. Closed-loop system with unity feedback.

When the complex perturbation 'f' deviates from 1, it indicates a departure from the nominal system behavior. In such cases, the closed-loop poles, which determine the stability of the system, may shift from the left-half plane (LHS) to the right-half plane (RHS) on the complex plane [25]. This movement of poles from the stable region to the unstable region signifies a degradation of system stability. The open-loop response under perturbation, denoted as f'$^*L$, represents the response of the system in the open-loop configuration when subjected to the complex perturbation (f). This response captures the effect of the perturbation on the behavior of the system. Consider a plot (see Fig. 6) that shows a disk in the complex plan.

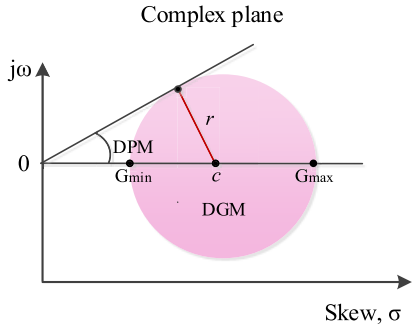

FIGURE 6. Closed-loop system with unity feedback.

The disk encircles the variations in relative gain in range of [G_{min}, G_{max}], and changes in absolute phase of DPM. The points where the disk intercepts the real axis determine the gain variation range DGM, while the angle formed by the real axis and a line passing through the origin and tangent to the disk determines the phase variation range DPM. The radius of the disk (r) corresponds to the amount of gain or phase variation that the system can tolerate without becoming unstable. If the feedback loop shown in Fig. 5 remains stable for all values of 'f', then disk-based gain margin of L is nearly equal to DGM from disk and disk-based phase margin of L is at least DPM. For SISO systems, the disk is parameterized by

$$\text{Multiplicative factor, f} = \frac{1+\frac{1-\sigma}{2}\delta}{1-\frac{1+\sigma}{2}\delta} : |\delta| < 1 \tag{10}$$

where δ is the normalized uncertainty. σ is the skew, and α is the disk size i.e. the weight of the gain and phase variations by perturbation f. The values of α and σ will be used to explain how a disk model changes in terms of gain and phase. The parameter σ regulates the gain variations as balance ($\sigma = 0$) and asymmetry ($\sigma \neq 0$), whereas the parameter α defines where the disk location on the real axis. The intercept values ($G_{\min}$, $G_{\max}$) on the disk real axis correlate to $\delta = \pm\alpha$ are given by

$$G_{min} = \frac{1+\left(\frac{1-\sigma}{2}\right)(-\alpha)}{1+\left(\frac{1+\sigma}{2}\right)(\alpha)} = \frac{2-(1-\sigma)\alpha}{2+(1+\sigma)\alpha} \tag{11}$$

$$G_{max} = \frac{1+\left(\frac{1-\sigma}{2}\right)(\alpha)}{1+\left(\frac{1+\sigma}{2}\right)(-\alpha)} = \frac{2+(1-\sigma)\alpha}{2-(1+\sigma)\alpha}$$

$$= 1/G_{min} \tag{12}$$

$$\text{Disk centre}(c) = \frac{G_{min}+G_{max}}{2} \tag{13}$$

$$\text{Disk radius } (r) = \frac{G_{max}-G_{min}}{2} \tag{14}$$

The variations in phase margin will depend on disk center (c) and disk radius (r). The peak phase variation

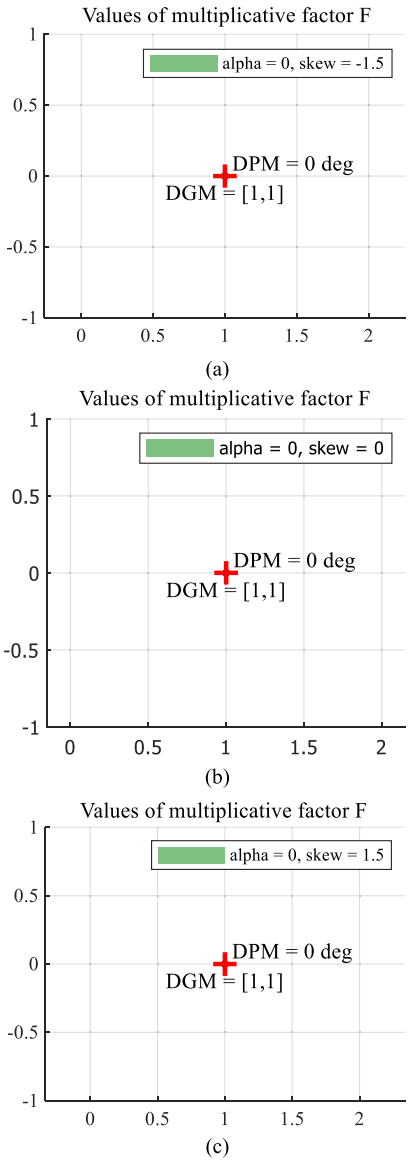

FIGURE 7. Values of multiple factor F for a) $\alpha = 0$ and skew $\sigma = -1.5$, b) $\alpha = 0$ and skew $\sigma = 0$,and c) $\alpha = 0$ and skew $\sigma = 1.5$.

$\varphi_m = \text{Sin}^{-1}(r/c)$, when the disk radius smaller than the disk center (i.e $r \leq c$). The φ_m is infinity when $r > c$. Consider the disk, for instance, with $\alpha = 0$ and skew $\sigma = 0$. On the disk, the intercept points are $G_{min} = 1$ and $G_{max} = 1$, the disk center and radius are 1 and 0 respectively. With these values, the plot of the disk with gain variation range DGM = [1 1], and DPM = 0^0 is as shown in Fig. 7 (b). This indicates that the gain variation range is symmetrical by a factor 1 of the nominal value. Similarly for $\alpha = 0$ and skew $\sigma = [-1.5\ 1.5]$, the plots of the disks with gain variation range DGM = [1 1] and DPM = 0^0 are as shown in Fig. 7 (a) and (c) respectively. In this case, also the range of the gain variations is symmetrical by a factor 1 of the nominal value. For the values of $\sigma < 0$ and $\sigma > 0$ with $\alpha = 0$, the phase margin obtained from the disk is 0^0. There should be at least a slight gain variation, when $\sigma < 0$ and $\sigma > 0$, to extract the phase margin from the disk. The variations in the gain will depend on the α value. The intercept points on the disk are G_{min}=0.33 and G_{max}=3 for α=1 and $\sigma = 0$. The disk radius is 1.335 and its center equals 1.665. With these values, the plot of the disk with gain variation range DGM= [0.33, 3] and DPM=53.3^0 is shown in Fig. 8 (b). Similarly for α=0 and $\sigma = [-1.5\ 1.5]$, the plot of the disks with gain variation range DGM and DPM are as depicted in Fig. 8 (a) and (c) respectively. The disk size should be large for the given value of σ to keep a closed loop system stable for all values of model perturbations according to (10) [29], [35].

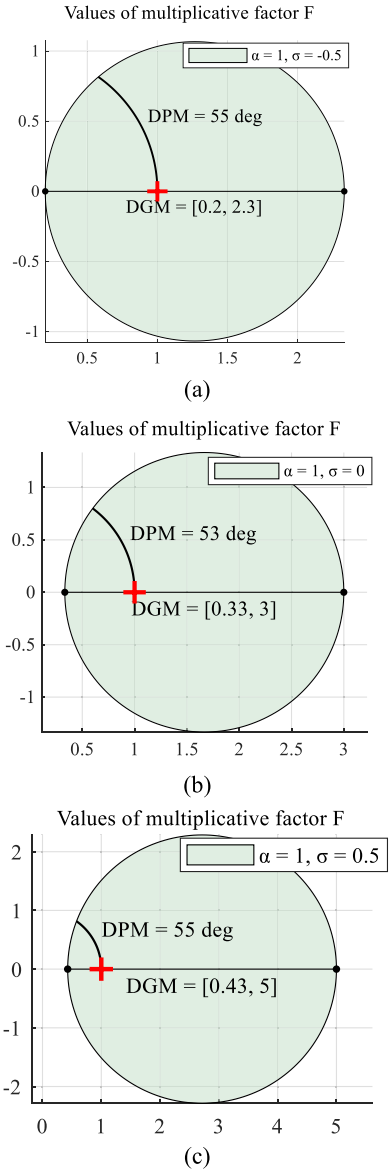

FIGURE 8. Values of multiple factor F for a) $\alpha = 1$ and skew $\sigma = -0.5$, b) $\alpha = 1$ and skew $\sigma = 0$, and c) $\alpha = 1$ and skew $\sigma = 0.5$.

V. SIMULATION RESULTS AND DISCUSSION

The simulation of the proposed work has been conducted using MATLAB (R2022b). The choice of MATLAB/Simulink as the simulation tool provides a robust

and widely-used platform for system modeling and analysis.

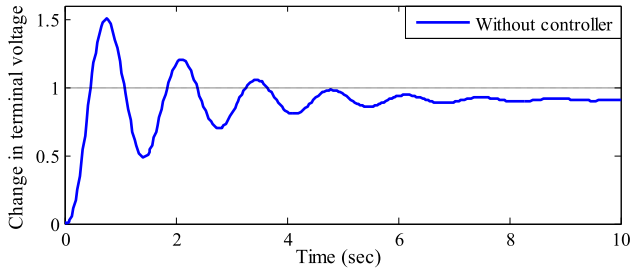

FIGURE 9. Simulated response of AVR without controller.

A. AVR STEP RESPONSE WITHOUT CONTROLLER

Fig. 9 shows the oscillatory response of the AVR system without the controller, for the given step input signal, with a peak overshoot of 1.505 pu and rise time (T_r) and settling time (T_s) of 0.437 and 6.99 sec respectively, and a stationary error of 0.091 pu. Also, Fig. 10 shows the bode plot of AVR system without the controller. Because of its extremely low DM (i.e. 0.0638 sec), the examined AVR system is less capable of stability in this case. Table 1 indicates the step response, closed loop poles, and frequency response of the AVR system without controller. According to Table 1, the AVR system is stable because all closed-loop poles and zeros are in the negative region of the pole-zero map.

TABLE 1. Performance of AVR without controllers.

Type of controller	Time response			Closed-loop system	
	%Os	T_r(s)	T_s(s)	Poles	Damping factor(ξ)
No controller	65.31	0.437	5.73	-100,-12.5 -0.51±4.66i	1 0.11

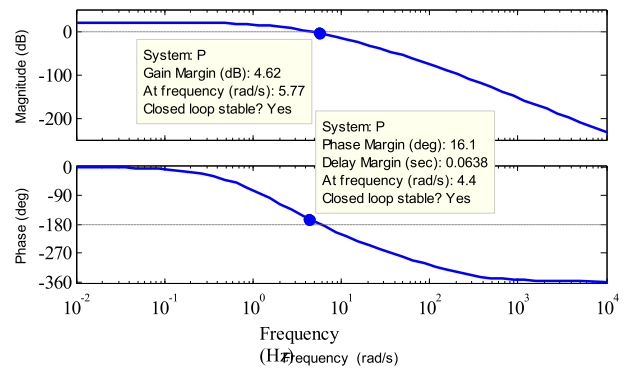

FIGURE 10. Frequency response of AVR without controller.

But, the presence of complex poles, -0.52 ± 4.66i, with low damping factor (ξ) indicates the potential for oscillatory behavior in the response of the system. In addition, the stability of the AVR system can be analyzed by computing the phase margin (PM). Typically, a phase margin of 45^0 or higher is desirable for a stable system. If the phase margin drops too low, this can lead to oscillations or instability in the system. Since the PM of the studied system was 16.1^0 (which is less than typical PM), the system was more oscillatory and became unstable for the given disturbances. To address this issue, a controller can be designed to provide additional damping and improve the phase margin of an AVR system. A well-designed controller can help stabilization of an AVR system, reduce oscillations, and enhance its transient response to disturbances.

B. AVR STEP RESPONSE WITH CONTROLLER

Fig. 11 shows the unit step response of the AVR system with PID controller. The performance of the AVR with the PID is summarized, in Table 2, in terms of its time response.

TABLE 2. Comparison of performance of AVR with controller.

Type of controller	Time response			Closed-loop system	
	%Os	T_r(s)	T_s(s)	Poles	ξ
NMR Algorithm (proposed)	9.07	0.182	0.906	-101.02 -0.19 ± 0.57i -5.75 ± 9.98i	1 0.902 0.712
TSA [19]	10.4	0.201	0.926	-101.55 -0.93 ± 0.82i -5.05 ± 11.32i	1 0.40 0.71
Improved Kidney-Inspired(IKI) [36]	15.01	0.128	0.753	-102 -0.80 ± 0.93i -5.13 ± 11.7i	1 0.65 0.40
AOA [14]	4.25	0.233	0.921	-100.75 -1.11 ± 0.89i -5.27 ± 7.05i	1 0.78 0.60
SA-MRFO [18]	1.88	0.241	1.83	-0.79; -1.57 -100.74, -5.20 ± 6.98i,	1 1 0.597

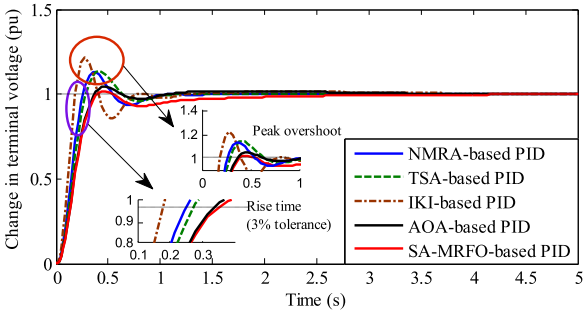

FIGURE 11. Comparison of AVR performance with various PID controllers.

Table 2 shows that all of the closed-loop poles are located in the left side of the complex plane, hence the AVR with the controller is stable. The AVR system with the NMRA-based controller exhibits superior transient response characteristics, such as low rise time, low settling time, and a larger damping factor compared to the TSA-PID, AOA-PID, and SA-MRFO-PID controllers. Furthermore, compared to the AOA-PID, SA-MRFO-PID, and IKI-PID controllers, the AVR system with NMRA-PID has a better transient response, with the exception of overshoot percent. Hence, the comparison in the rest of the article is primarily focused on comparing the proposed NMRA-PID controller with the TSA-PID controller,

rather than the AOA-PID, SA-MRFO-PID, and IKI-PID controllers.

Fig. 12 shows the comparison plot for voltage error applied to the NMRA-based PID and TSA-based PID controller.

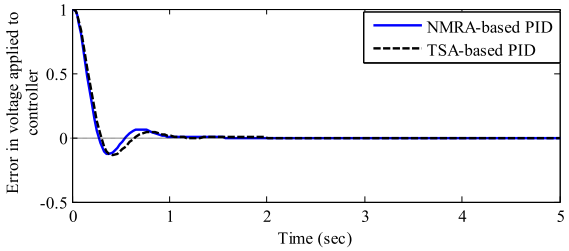

FIGURE 12. Comparison of voltage error applied to controller.

The frequency response for AVR with NMRA-PID and TSA-PID controller, is depicted in Fig. 13, which presumably shows the gain of the system as a function of frequency.

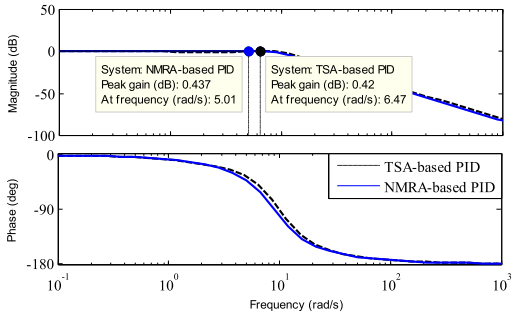

FIGURE 13. Comparison of frequency response of AVR with NMRA-PID and TSA-PID controllers.

C. DISK MARGINS OF STUDIED AVR

For the given a loop transfer function L and a skew value σ, the disk margin represents the disk size α such that the closed-loop system remains stable for all values of 'f' within that disk.

1) SKEW$\sigma = 0$

The disk size α of the AVR system with the proposed controller is computed as 0.924 for σ=0. Fig. 14 displays the plot for the values of perturbation in the AVR system's feedback loop or multiplicative factor for $\alpha = 0.924$ and σ=0, and Table 3 lists the relevant DGM variations.

This indicates that the system remains stable for relative changes in gain [0.37 2.72] of its nominal gain. However, in practical scenarios, the AVR system can experience simultaneous variations in both gain and phase. The stable range of combined gain and phase variations is visualized in Fig. 15, where the shaded region represents the range of stable operation.

Since there is no phase variation considered in the initial analysis, it is stated that without phase variation, the AVR system with the NMRA-PID controller can tolerate a gain variation of ±8.68 dB within the full range of DGM. This

TABLE 3. DGM and DPM variations, tolerable gain variation of AVR with NMRA-PID controller.

Disk size, Skew	NMRA-PID (proposed) Controller				
	Disk radius	Disk center	DGM variation	DPM variation	Tolerable Gain variation*
$\alpha = 0.924$, $\sigma = 0$	1.165	1.535	[0.37, 2.7]	$\pm 50^0$	±8.68dB
$\alpha = 0.924$, $\sigma = -0.5$	1.077	1.272	[0.195, 2.35]	$\pm 55^0$	[-14.20,9.45]*
$\alpha = 0.924$, $\sigma = 0.5$	1.234	1.736	[0.502, 2.97]	$\pm 44.1^0$	

* No phase variation

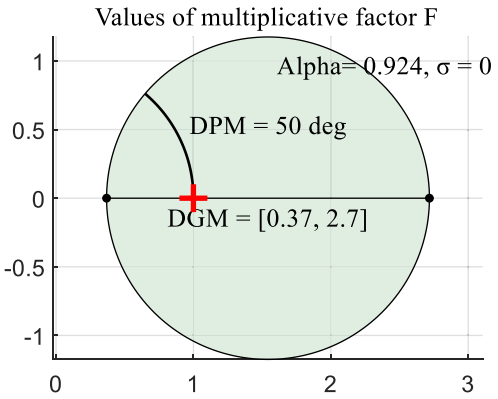

FIGURE 14. Values of multiplicative factor for $\alpha = 0.924$ and $\sigma = 0$(AVR system with NMRA-based PID controller).

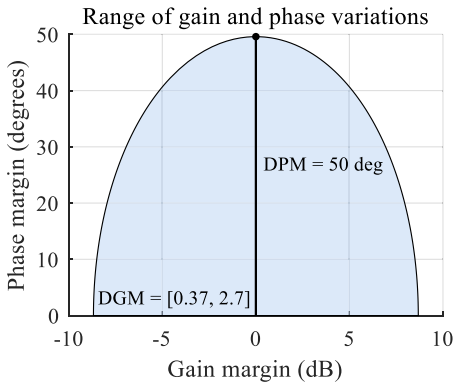

FIGURE 15. Gain and phase variations for $\alpha = 0.924$ and $\sigma = 0$(AVR system with NMRA-based PID controller).

implies that the system remains stable for relative changes in gain up to ±8.68 dB. Similarly, the disk size α of the AVR system with the TSA-PID controller is computed as 0.85. Fig. 16 displays the plot for the values of perturbation in the AVR system's feedback loop or multiplicative factor for $\alpha = 0.85$ and $\sigma = 0$, and Table 4 lists the relevant DGM variations. The disk-based gain margin (DGM) variation for the AVR system with the TSA-PID controller is in the range of [0.4, 2.5].

These analyses provide insights into the stability and robustness of the AVR system under different controllers and perturbation scenarios. It seems that the NMRA-PID controller allows for a wider range of gain variations

TABLE 4. DGM and DPM variations, tolerable gain variation of AVR with TSA-PID controller.

Disk size, Skew	TSA-PID Controller				
	Disk radius	Disk center	DGM variation	DPM variation	Tolerable Gain variation*
$\alpha = 0.85$, $\sigma = 0$	1.05	1.45	[0.4, 2.5]	$\pm 46^0$	±7.88dB
$\alpha = 0.85$, $\sigma = -0.5$	0.975	1.225	[0.25, 2.20]	$\pm 50.9^0$	
$\alpha = 0.85$, $\sigma = 0.5$	1.068	1.592	[0.524, 2.66]	$\pm 41.3^0$	[-12.10, 8.51]*

* No phase variation

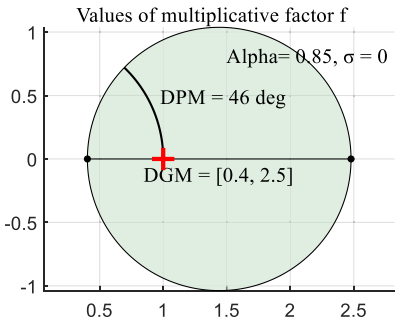

FIGURE 16. Values of multiplicative factor for $\alpha = 0.85$ and $\sigma = 0$(AVR system with TSA-based PID controller).

compared to the TSA-PID controller in the absence of phase variations, $\sigma = 0$. This means that the system remains stable for relative changes in gain between 0.4 and 2.5 times of its nominal gain. Considering the presence of simultaneous gain and phase variations, the stable range of combined gain and phase variations for the AVR system with the TSA-PID controller is visualized in Fig.17, where the shaded region represents the range of stable operation. Since there is no phase variation considered, the AVR system with the TSA-PID controller can tolerate a gain variation of ±7.88 dB within the full range of DGM.

2) SKEW$\sigma = \pm 0.5$

The disk-based gain margin (DGM) variation, for AVR with proposed controller, is in the range of [0.195, 2.35] and phase variation (DPM) is $\pm 55^0$ for $\sigma = -0.5$, and the corresponding values for $\sigma = 0.5$ are [0.502, 2.97] and $\pm 44.10^0$ respectively. The plots for the values of perturbation in the feedback loop of the AVR system for $\alpha = 0.924$ and $\sigma = \pm 0.5$ are shown in Fig. 18. The corresponding DGM variations are listed in Table 3. The range of combined gain and phase variations is shown in Fig. 19, where the shaded region represents the range of stable operation.

This implies that the system remains stable for relative changes in gain range of $[-14.20, 9.45]$ dB. Similarly, the disk-based gain margin (DGM) variation, for AVR with TSA-PID controller, is in the range of [0.25, 2.20], and phase variation (DPM) is $\pm 50.9^0$ for $\sigma = -0.5$, and the corresponding values for $\sigma = 0.5$ are [0.524, 2.66] and $\pm 41.30^0$ respectively. The plots for the values of multiplicative factor

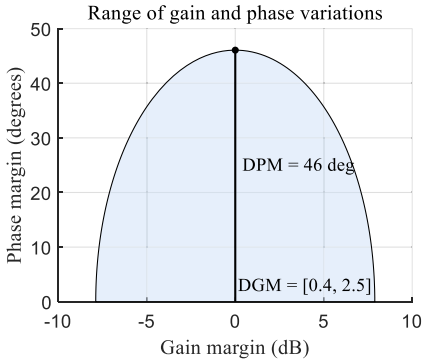

FIGURE 17. Gain and phase variations for $\alpha = 85$ and $\sigma = 0$ (AVR system with TSA-based PID controller).

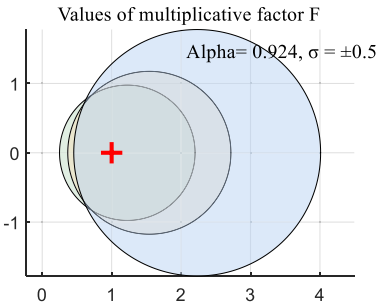

FIGURE 18. Values of multiplicative factor for $\alpha = 0.924$ and $\sigma = \pm 0.5$ (AVR system with NMRA-based PID controller).

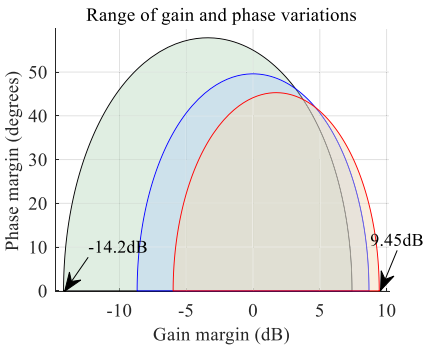

FIGURE 19. Gain and phase variations for $\alpha = 0.924$ and $\sigma = \pm 0.5$ (AVR system with NMRA-based PID controller).

in the feedback loop of the AVR system for $\alpha = 0.85$ and $\sigma = \pm 0.5$ are shown in Fig. 20. The corresponding DGM variations are listed in Table 4. The range of combined gain and phase variations is shown in Fig. 21, where the shaded region represents the range of stable operation. This implies that the system remains stable for relative changes in gain range of $[-12.10, 8.51]$ dB.

These results provide a detailed understanding of the stability and robustness of the AVR system. The visual representations and ranges of stable operation give valuable insights into the system's behavior and its ability to handle variations in gain and phase.

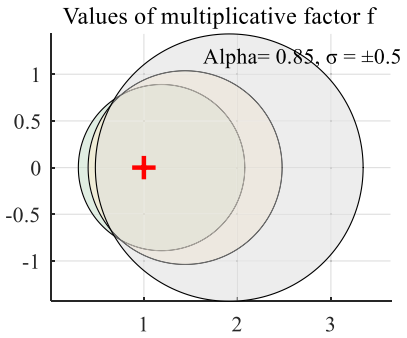

FIGURE 20. **Values of multiplicative factor for $\alpha = 0.85$ and $\sigma = \pm 0.5$(AVR system with TSA-based PID controller).**

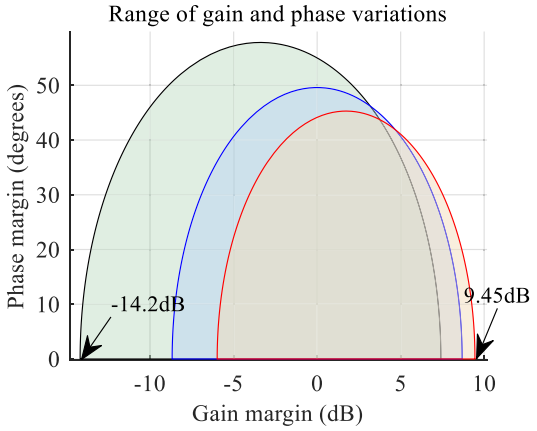

FIGURE 21. **Gain and phase variations for $\alpha = 0.85$ and $\sigma = \pm 0.5$(AVR system with TSA-based PID controller).**

The DGM and DPM variations of the AVR system with NMRA-PID and TSA-PID controllers are listed in Tables 3 and 4 for various values of disk size and skew.

D. CONTROLLER STABILITY AND ROBUSTNESS

It is believed that the AVR system with the NMRA-based controller will be more stable than the AVR system with the TSA-PID controller because the peak gain provided by the NMRA-PID controller is greater than the peak gain provided by the TSA-PID controller, (see Fig. 11).

For the specified value of skew, the disk size should be large in order to maintain the stability of the closed loop system for all values of model perturbations. For the specified value of skew (i.e., 0 or ± 0.5) in this study, the disk size of the AVR with NMRA-PID controller is 0.924, while the disk size of the AVR with TSA-PID controller is 0.85.The AVR system with the NMRA-based controller is more reliable since it offers a larger disk size than the TSA-PID controller.

Table 3 clearly shows that for the given perturbations or multiplicative factor ($\sigma = 0$) in the feedback loop of the AVR system, the proposed NMRA-PID controller has a higher gain change tolerance than the TSA-PID controller. The specified tolerance for gain adjustments for the NNRA-PID controller is ± 8.68 dB, but the listed tolerance for the TSA-PID controller is ± 7.88 dB. As a result, it can be seen that the performance of the recommended NMRA-PID controller is not significantly affected by larger swings in system gain. Additionally, Table 3 also shows that the recommended controller is more robust, for the given perturbations or multiplicative factor, than the TSA-PID controller for $\sigma = \pm 0.5$.

VI. CONCLUSION

The study introduces a novel tuning method called the Naked Mole Rat algorithm (NMRA) and investigates its application in designing PID controllers for automatic voltage regulator (AVR) systems. According to Table 2 in the study, all of the closed-loop poles of the AVR system with the NMRA-based controller are located in the left side of the complex plane. This implies that the AVR system, when combined with the NMRA-based controller, is stable. Furthermore, the AVR system with NMRA-based controller demonstrates superior transient response compared to other controller designs. Specifically, it exhibits low rise time, low settling time, and a larger damping factor when compared to the TSA-PID, AOA-PID, and SA-MRFO-PID controllers.

The study highlights the limitations of conventional stability analysis techniques, such as the Bode plot, in the frequency domain. While the Bode plot can determine the GM and PM of the AVR system including the PID controller, it may not provide the minimum GM and PM required for a thorough stability analysis. To overcome these limitations, the article suggests utilizing disk-based margins for stability. This approach is proposed as a more reliable alternative that can mitigate the shortcomings of conventional stability analysis.

For the specified value of skew, the disk sizes of the AVR system with the NMRA-PID and TSA-PID controllers are reported as 0.924 and 0.85 respectively. The larger disk size of the AVR system with the NMRA-PID controller indicates that it has a higher tolerance to model perturbations and possesses more stability for various perturbation values. The AVR with proposed controller shows a gain change tolerance of ± 8.68 dB, while the TSA-PID controller has ± 7.88 dB. This suggests that the performance of the NMRA-PID controller is less affected by larger variations in system gain compared to the TSA-PID controller. From the reported results, the NMRA-PID controller provides a larger disk size, higher gain change tolerance, and increased robustness compared to the TSA-PID controller.

The future work of this study is aims to comprehensively analyze the performance of AVR systems by considering the nonlinearities (e.g. time delays of exciter or generator and saturation of transformer). The proposed algorithm could be implemented in Automatic Generation Control, Power System Stabilizer, and DG placement in radial distribution system. This study not only enhances the understanding of AVR behavior but also provides valuable guidance for future research and practical implementations in power systems.

REFERENCES

[1] M. Mahdavi, K. Schmitt, and F. Jurado, "Robust distribution network reconfiguration in the presence of distributed generation under uncertainty in demand and load variations," *IEEE Trans. Power Del.*, vol. 38, no. 5, pp. 3480–3495, Oct. 2023, doi: 10.1109/TPWRD.2023.3277816.

[2] H. M. Hasanien, "Design optimization of PID controller in automatic voltage regulator system using Taguchi combined genetic algorithm method," *IEEE Syst. J.*, vol. 7, no. 4, pp. 825–831, Dec. 2013, doi: 10.1109/JSYST.2012.2219912.

[3] P. Gopi, M. Ramesh, and M. P. Lalitha, "Evaluation of automatic voltage regulator's PID controller coefficients using Python," in *Proc. IEEE Madras Sect. Conf. (MASCON)*, Virtual, India, Aug. 2021, pp. 1–7.

[4] M. Ćalasan, M. Micev, Ž. Djurovic, and H. M. A. Mageed, "RETRACTED: Artificial ecosystem-based optimization for optimal tuning of robust PID controllers in AVR systems with limited value of excitation voltage," *Int. J. Electr. Eng. Educ.*, vol. 60, no. 1, pp. 1857–1884, Jul. 2020, doi: 10.1177/0020720920940605.

[5] K. H. Ang, G. Chong, and Y. Li, "PID control system analysis, design, and technology," *IEEE Trans. Control Syst. Technol.*, vol. 13, no. 4, pp. 559–576, Jul. 2005, doi: 10.1109/TCST.2005.847331.

[6] J. G. Ziegler and N. B. Nichols, "Optimum settings for automatic controllers," *Trans. ASME*, vol. 64, no. 8, pp. 759–765, Nov. 1942, doi: 10.1115/1.4019264.

[7] A. Jalilvand, A. Kimiyaghalam, A. Ashouri, and M. Mahdavi, "Advanced particle swarm optimization-based PID controller parameters tuning," in *Proc. IEEE Int. Multitopic Conf.*, Karachi, Pakistan, Dec. 2008, pp. 429–435, doi: 10.1109/INMIC.2008.4777776.

[8] P. Gopi et al., "Dynamic behavior and stability analysis of automatic voltage regulator with parameter uncertainty," *Int. Trans. Electr. Energy Syst.*, vol. 2023, pp. 1–13, Jan. 2023, doi: 10.1155/2023/6662355.

[9] S. Panda, B. K. Sahu, and P. K. Mohanty, "Design and performance analysis of PID controller for an automatic voltage regulator system using simplified particle swarm optimization," *J. Franklin Inst.*, vol. 349, no. 8, pp. 2609–2625, Oct. 2012, doi: 10.1016/j.jfranklin.2012.06.008.

[10] Z.-L. Gaing, "A particle swarm optimization approach for optimum design of PID controller in AVR system," *IEEE Trans. Energy Convers.*, vol. 19, no. 2, pp. 384–391, Jun. 2004, doi: 10.1109/TEC.2003.821821.

[11] N. Nahas, M. Abouheaf, A. Sharaf, and W. Gueaieb, "A self-adjusting adaptive AVR-LFC scheme for synchronous generators," *IEEE Trans. Power Syst.*, vol. 34, no. 6, pp. 5073–5075, Nov. 2019, doi: 10.1109/TPWRS.2019.2920782.

[12] A. Abbasy and S. H. Hosseini, "Ant colony optimization-based approach to optimal reactive power dispatch: A comparison of various ant systems," in *Proc. IEEE Power Eng. Soc. Conf. Expo. Afr.-Power Africa*, South Africa, Jul. 2007, pp. 1–8, doi: 10.1109/PESAFR.2007.4498067.

[13] A. M. Mosaad, M. A. Attia, and A. Y. Abdelaziz, "Comparative performance analysis of AVR controllers using modern optimization techniques," *Electr. Power Compon. Syst.*, vol. 46, nos. 19–20, pp. 2117–2130, Dec. 2018, doi: 10.1080/15325008.2018.1532471.

[14] T. Dogruer and M. S. Can, "Design and robustness analysis of fuzzy PID controller for automatic voltage regulator system using genetic algorithm," *Trans. Inst. Meas. Control*, vol. 44, no. 9, pp. 1862–1873, Jan. 2022, doi: 10.1177/014233122110667.

[15] M. Micev, M. Ćalasan, D. Stipanović, and M. Radulović, "Modeling the relation between the AVR setpoint and the terminal voltage of the generator using artificial neural networks," *Eng. Appl. Artif. Intell.*, vol. 120, Apr. 2023, Art. no. 105852, doi: 10.1016/j.engappai.2023.105852.

[16] A. Agwa, S. Elsayed, and M. Ahmed, "Design of optimal controllers for automatic voltage regulation using archimedes optimizer," *Intell. Autom. Soft Comput.*, vol. 31, no. 2, pp. 799–815, Sep. 2022, doi: 10.32604/iasc.2022.019887.

[17] D. Izci, S. Einci, and S. Mirjalili, "Optimal PID plus second-order derivative controller design for AVR system using a modified Runge Kutta optimizer and bode's ideal reference model," *Int. J. Dyn. Control.*, vol. 11, no. 3, pp. 1247–1264, Oct. 2022, doi: 11.10.1007/s40435-022-01046-9.

[18] D. Izci, S. Ekinci, H. Zeynelgil, and J. Hedley, "Fractional order PID design based on novel improved slime mould algorithm," *Electr. Power Compon. Syst.*, vol. 49, pp. 901–918, Jun. 2022, doi: 10.1080/153250.08.2022.2049650.

[19] S. Ekinci, D. Izci, and B. Hekimoglu, "Henry gas solubility optimization algorithm based FOPID controller design for automatic voltage regulator," in *Proc. Int. Conf. Electr., Commun., Comput. Eng. (ICECCE)*, Istanbul, Turkey, Jun. 2020, pp. 1–6, doi: 10.1109/ICECCE49384.2020.9179406.

[20] M. Micev, M. Ćalasan, Z. M. Ali, H. M. Hasanien, and S. H. E. A. Aleem, "Optimal design of automatic voltage regulation controller using hybrid simulated annealing—Manta ray foraging optimization algorithm," *Ain Shams Eng. J.*, vol. 12, no. 1, pp. 641–657, Mar. 2021, doi: 10.1016/j.asej.2020.07.010.

[21] E. Köse, "Optimal control of AVR system with tree seed algorithm-based PID controller," *IEEE Access*, vol. 8, pp. 89457–89467, 2020, doi: 10.1109/ACCESS.2020.2993628.

[22] A. M. Mosaad, M. A. Attia, and A. Y. Abdelaziz, "Whale optimization algorithm to tune PID and PIDA controllers on AVR system," *Ain Shams Eng. J.*, vol. 10, no. 4, pp. 755–767, Dec. 2019, doi: 10.1016/j.asej.2019.07.004.

[23] M. Mahdavi, A. Kimiyaghalam, H. H. Alhelou, M. S. Javadi, A. Ashouri, and J. P. S. Catalão, "Transmission expansion planning considering power losses, expansion of substations and uncertainty in fuel price using discrete artificial bee colony algorithm," *IEEE Access*, vol. 9, pp. 135983–135995, 2021, doi: 10.1109/ACCESS.2021.3116802.

[24] C. N. Sai Kalyan, A. K. B. S. Goud, H. Pulluri, P. Gopi, and B. Sekhar, "Falcon optimization algorithm based regulator for the study of automatic load frequency control," in *Proc. 3rd Int. Conf. Commun., Comput. Ind. (CI)*, Bengaluru, India, Dec. 2022, pp. 1–6.

[25] C. N. S. Kalyan, P. Gopi, C. R. Reddy, Y. Belkhier, M. Bajaj, and R. N. Shaw, "Integral double derivative plus filter controller for frequency regulation of dual area power system with HVDC line," in *Proc. IEEE IAS Global Conf. Renew. Energy Hydrogen Technol. (GlobConHT)*, Male, Maldives, Mar. 2023, pp. 1–6, doi: 10.1109/GlobConHT56829.2023.10087776.

[26] V. Padiachy, U. Mehta, S. Azid, S. Prasad, and R. Kumar, "Two degree of freedom fractional PI scheme for automatic voltage regulation," *Eng. Sci. Technol., Int. J.*, vol. 30, Jun. 2022, Art. no. 101046, doi: 10.1016/j.jestch.2021.08.003.

[27] M. A. Siddiqui, M. Anwar, S. Laskar, M. Shamsuzzoha, and M. Mahboob, "Closed loop tuning of cascade controllers based on setpoint experiment," *J. Eng. Res.*, vol. 8, no. 4, pp. 117–138, Dec. 2020, doi: 10.36909/jer.v8i4.8492.

[28] M. Mahdavi, H. H. Alhelou, P. Siano, and V. Loia, "Robust mixed-integer programing model for reconfiguration of distribution feeders under uncertain and variable loads considering capacitor banks, voltage regulators, and protective relays," *IEEE Trans. Ind. Informat.*, vol. 18, no. 11, pp. 7790–7803, Nov. 2022, doi: 10.1109/TII.2022.3141412.

[29] P. Seiler, A. Packard, and P. Gahinet, "An introduction to disk margins [lecture notes]," *IEEE Control Syst. Mag.*, vol. 40, no. 5, pp. 78–95, Oct. 2020, doi: 10.1109/MCS.2020.3005277.

[30] P. Gopi, S. Srinivasan, and M. Krishnamoorthy, "Disk margin based robust stability analysis of a DC motor drive," *Eng. Sci. Technol., Int. J.*, vol. 32, Aug. 2022, Art. no. 101074, doi: 10.1016/j.jestch.2021.10.006.

[31] M. Furat and G. G. Cücü, "Design, implementation, and optimization of sliding mode controller for automatic voltage regulator system," *IEEE Access*, vol. 10, pp. 55650–55674, 2022, doi: 10.1109/ACCESS.2022.3177621.

[32] T. A. Lipo, *Analysis of Synchronous Machines*, 2nd ed. Boca Raton, FL, USA: Taylor & Francis, 2017, pp. 1–590.

[33] H. Saadat, *Power System Analysis*. New York, NY, USA: McGraw-Hill, 2002.

[34] R. Salgotra and U. Singh, "The naked mole-rat algorithm," *Neural Comput. Appl.*, vol. 31, no. 12, pp. 8837–8857, Sep. 2019, doi: 10.1007/s00521-019-04464-7.

[35] J. D. Blight, R. L. Dailey, and D. Gangsaas, "Practical control law design for aircraft using multivariable techniques," *Int. J. Control*, vol. 59, no. 1, pp. 93–137, Jan. 1994, doi: 10.1080/00207179408923071.

[36] S. Ekinci and B. Hekimoglu, "Improved kidney-inspired algorithm approach for tuning of PID controller in AVR system," *IEEE Access*, vol. 7, pp. 39935–39947, 2019, doi: 10.1109/ACCESS.2019.2906980.